Global Spatial Distribution of Hack's Law Exponent on Mars and its Early Climate

W. Luo[1], A. D. Howard[2], R. A. Craddock[3], E. Oliveira[4], R. Pires[4]

[1]Northern Illinois University, DeKalb, IL, USA

[2]Planetary Science Institute, Tucson, AZ, USA

[3]Smithsonian Institution, Washington, DC, USA

[4]University of Fortaleza, Fortaleza, Ceará, Brazil

Corresponding author: Wei Luo (`wluo@niu.edu`)

Key Points:

- A parameter free Invasion Percolation Based Algorithm is adapted to delineate watersheds draining to mapped valley networks on Mars
- Statistical analysis of Hack's Law exponent show clustered distribution, suggesting regional variations in controlling factors/processes
- The mean value of Hack's Law exponent is most similar to that of arid regions on Earth, implying an early arid climate on Mars

Abstract

Widespread valley networks (VNs) on Mars and other evidence point to an early warm and wet climate. However, ongoing debates still exist about VN's formation processes and climate conditions. The power law relationship between basin length and area (Hack's Law) can be diagnostic of different fluvial processes and thus climate conditions. Past studies of Hack's Law on Mars at local sites have produced inconclusive results. Here we used a parameter free method to delineate watersheds globally on Mars based on mapped VNs and then extracted their Hack's Law exponent (h). Spatial statistical analyses show that the spatial distribution of h on Mars is not random but with clustered high and low values, suggesting regional variations in controlling factors/processes responsible for VN formation. The majority of h values on Mars are most similar to values related to arid climates on Earth, implying similar conditions for early Mars.

Plain Language Summary

Valley networks on Mars are river-valley-like features distributed primarily across the ancient cratered highland terrains. There are still debates on how they were formed and under what climate conditions. We adapted an algorithm that only requires mapped valley network and topography data as input to extract drainage basins on Mars and examined the relationship between valley network length and drainage area (known as Hack's Law). We found this relationship to be similar to terrestrial watersheds formed in arid regions of the Earth. Our results indicate that a majority of Martian valley networks were formed by precipitation in an arid climate.

1 Introduction

Valley networks (VNs) on Mars are river-valley-like features distributed primarily across the ancient cratered terrains. These features are widely interpreted as a record of past fluvial erosion, implying prolonged running liquid water across the surface and warm and wet early climate (e.g., Craddock & Howard, 2002; Hynek & Phillips, 2003; Luo & Stepinski, 2009; Ramirez & Craddock, 2018a). However, some climate models have difficulties in producing the necessary warm and wet conditions because Mars is in an orbit farther away from the Sun, thus it receives only about 43% of the solar energy that Earth does. In addition, the Sun's luminosity 3.8 billion years ago (when most of the VNs were believed to be formed) was only ~70% of its present value (Gough, 1981). This has led to many debates about VN's formation processes and early Mars climate conditions. For example, it may have been that the early climate of Mars was only episodically warm and wet created by brief and strong volcanic activity and associated outgassing of greenhouse gasses and aerosols (Halevy & Head, 2014); VNs were formed by groundwater sapping associated with magma intrusion and hydrothermal activities, thus not requiring continuous warm and wet conditions (Gulick, 1998); VNs could be created during short-lived episodes of top-down melting of thick cold-based ice on the equatorial highlands (Fastook & Head, 2015; Forget et al., 2013; R. Wordsworth et al., 2013; R. D. Wordsworth, 2016a) or localized basal melting and erosion by subglacial flows (e.g., Buffo et al., 2022; Grau Galofre et al., 2020, 2022). Scientists are still debating which climatic scenario is correct and whether non-runoff alternatives can create the observed valley networks (Baker et al., 2015; Ehlmann et al., 2011; Ramirez et al., 2020; Ramirez & Craddock, 2018b; Turbet & Forget, 2019; R. D. Wordsworth, 2016b).

Quantitative morphometric analysis of the landforms at basin scales can provide valuable information to determine (and thus test) past processes and climatic conditions. Hack's Law exponent is one such morphometric measure. Here we report a global scale analysis of Hack's Law exponent on Mars in comparison with terrestrial analysis in the conterminous US and draw the implications for early Mars climate.

Hack's Law is an empirical power law relationship between drainage basin area and the length of the main stream channel (Hack, 1957):

$$L = \mathrm{kA}^{h} \quad (1)$$

where L is the length from a locality on a stream to the drainage divide measured along the channel of the longest stream above that locality; A is the area of the basin that drain to the same locality; h is the Hack's exponent; and k is a constant. Theoretically, for self-similar networks, $h = 0.5$ (Dodds & Rothman, 2000). In general, h 0.5–0.6 are expected for fluvial systems (e.g., Hack, 1957; Penido et al., 2013; Rigon et al., 1993), implying that watersheds are slightly elongated downstream. Yi et al. (2018) found that the Hack's exponent is also related to climate (aridity). In arid areas, h is roughly 0.5, whereas in humid areas h is approximately 0.6. This is related to the groundwater involvement in

the valley development in humid regions (Yi et al., 2018).

A number of studies have examined the Hack's Law exponent for selected VN systems or basins on Mars. For example, Som et al. (2009) examined 10 large VN systems and found that h ranges from 0.47 to 19.2, in contrast to the narrower terrestrial range of 0.5-0.6. Caprarelli & Wang (2012) obtained h value of 1.02 for Evros Vallis. Penido et al. (2013) studied a number of selected small VN systems based on HRSC DEM data and found $h = 0.56 \sim 0.89$ with a median value of 0.74. Ansan and Mangold (2013) analyzed 13 selected basins and found $h = 0.47 \sim 0.78$. However, these previous studies have only looked at various selected areas, we are not aware of any a global comprehensive study on the distribution of Hack's Law exponent on Mars. Our study intends to fill this gap.

2 Materials and Methods

2.1 Data

For Earth (conterminous US), we used the SRTM 90-m Digital Elevation Database v4.1 (Jarvis et al., 2008), which is the enhanced version from the original NASA Shuttle Radar Topographic Mission (SRTM) data and is well suited for continental scale applications. For watershed boundary delineation, we used the Watershed Boundary Dataset (WBD), which is a seamless, national hydrologic unit dataset (https://www.usgs.gov/national-hydrography/watershed-boundary-dataset), and we selected the HUC6 (USGS hydrologic unit) basins because this level of watersheds provide the reasonable size and resolution for a continental scale analysis and this level is also used in other similar studies (e.g., Yi et al. 2018). We also utilized Global Aridity Index and Potential Evapotranspiration Climate Database (Trabucco, Antonio & Zomer, Robert, 2022). For Mars, we used MOLA DEM at 463 m resolution (Smith et al., 2001) and the HRSC and MOLA Blended Digital Elevation Model at 200 m (Fergason et al., 2018). We also used the mapped VN (Matsubara et al., 2013) while delineating the watershed boundaries using the IPBA algorithm as described below.

2.2 Watershed delineation

Delineating the watershed boundary is the first step for deriving Hack's law exponent. For terrestrial analysis, the standard technique is to use a flow-based method to extract watershed boundary from a digital elevation model (DEM) (usually implemented in GIS software), which involves filling the depressions in the DEM to make it drainable, deriving flow direction based on the steepest descent (D8 algorithm), and finding the flow accumulation along flow direction as the cumulative number of upstream cells flowing into each cell. The flow accumulation above a certain threshold defines the valley network, and cells draining into each valley network are grouped as the watershed (e.g., O'Callaghan & Mark, 1984). However, the flow-based method is designed for processing Earth data, and it is notoriously difficult to apply to Mars due to the disruptions and fragmentations of topography by impact cratering that post-date valley network

formation. The arbitrarily chosen flow accumulation threshold can easily result in stream networks that are over- or under-extracted, and tedious human intervention is often necessary to remove spurious results (e.g., Ansan & Mangold, 2013; Mest et al., 2010; Stepinski & Coradetti, 2004).

Alternatively, the Invasion Percolation-Based Algorithm (IPBA) is a parameter free algorithm that is robust and efficient and well suited for cratered topography (Fehr et al., 2009; Oliveira et al., 2019; Wilkinson & Willemsen, 1983). Invasion Percolation (IP) was originally designed to simulate one fluid displacing another from a porous medium under the action of capillary forces (Wilkinson & Willemsen, 1983), but it has been successfully applied to delineate watershed (Fehr et al., 2009; Oliveira et al., 2019). This works because in principle IP be applied to any process which proceeds along a path of least resistance (Wilkinson & Willemsen, 1983) and the fluvial processes that form watersheds also follow least resistance path (steepest descent downhill). We adapted this algorithm for our purpose of delineating watershed draining to mapped VNs (or streams) by first converting the VN (stream) vector lines as raster cells and the raster cells representing the valley (stream) line receive the same valley (stream) line ID as their cell value. Given a regular elevation grid (DEM) and a set of sinks S (streams or valleys), the IPBA sequentially applies the traditional IP algorithm over all cells of the grid, starting from a source cell (i.e., a seed cell) to form an invaded cluster. The growth dynamics iteratively add *the lowest of the neighboring cells* to the cluster (i.e., growing the cluster by invading the surrounding cells). The invaded cluster grows until it reaches a sink cell (or a cell that was once part of an invaded cluster in any previous IP iterations) and the invaded cluster is labeled with the ID of the sink cell (or the ID of the cluster already labeled). When two clusters with different labels meet, the contact edge is then marked as the watershed boundary between them. Therefore, the cells with the same ID belong to the same watershed since they are connected to the same valley (stream). Fig. 1 shows how IPBA is applied in topographic profile form with two sink cells, given four random source cells. The python code for this version of IPBA is available on GitHub (https://github.com/erneson/IPBA).

An intuitive way to understand the idea behind the IPBA is to consider a simple flooding model (Fehr et al., 2009). The model gradually increases flood level at each iteration, cells under water form unlabeled clusters and grow over the landscape. The unlabeled clusters are only labeled when they touch a sink cell. These labels stand until the end of the process. The watershed boundary is defined by the interface line between two labeled clusters. This model is a slightly adjusted version of a well-known watershed algorithm for image segmentation (Vincent & Soille, 1991). It was already shown that the IPBA is mathematically equivalent to the flooding model, but IPBA is more time efficient (Fehr et al., 2009).

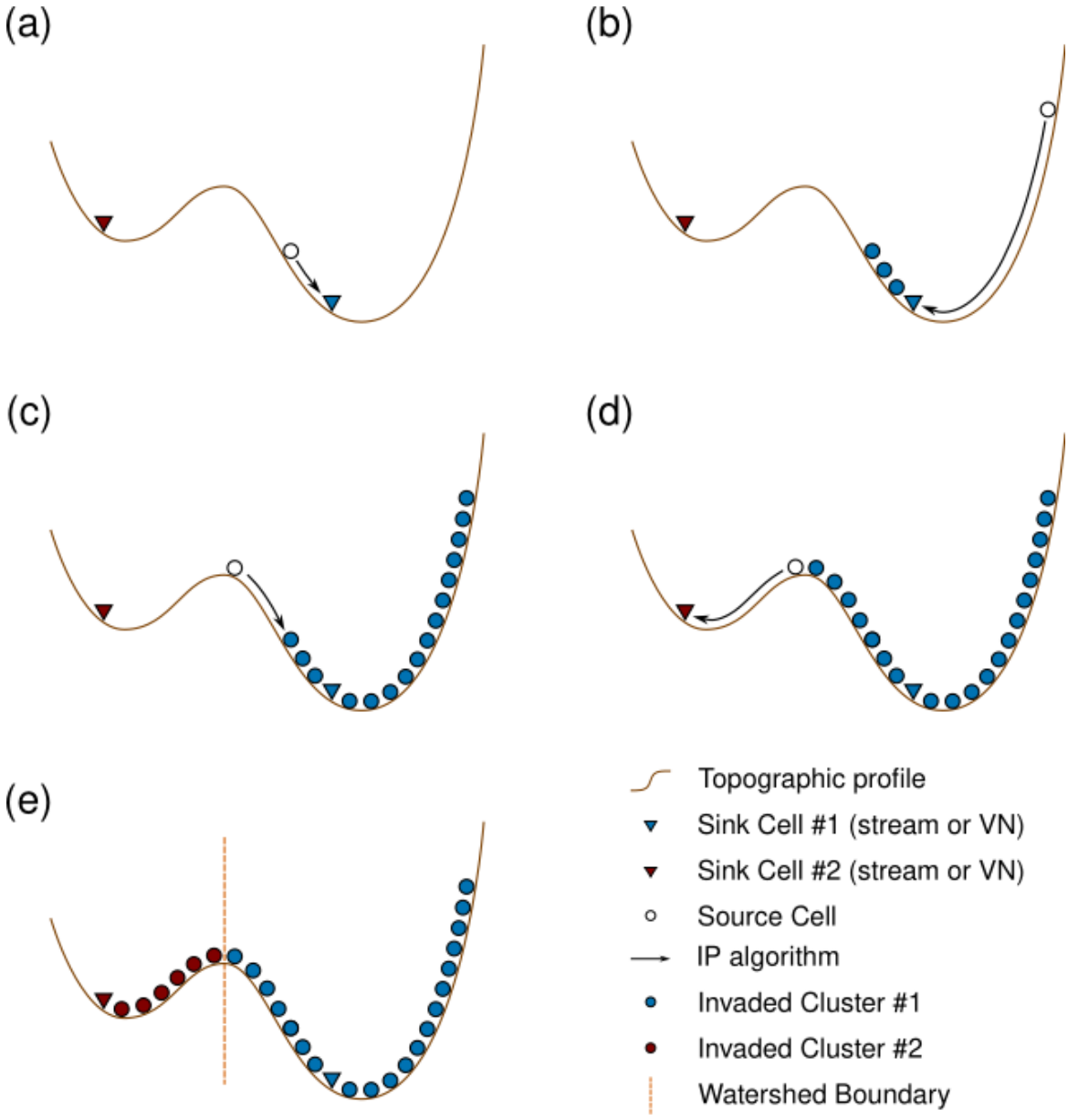

Figure 1: Illustration of the IPBA algorithm on a topographic profile. In (a), we apply the traditional IP algorithm starting from a source cell (white circle) and invading neighboring cells that are *lower* than source cell elevation until it reaches a sink cell, by doing so we form an invaded cluster shown by blue circles in (b). The process repeats starting from different source cells (white circles) in (b) and (c). Also, in (c), we show the case where the invaded cluster reaches a cell that is part of an invaded cluster in a previous IPBA interaction. In (d) and

(e), we show the result of the IP algorithm starting from a source cell that after the invasion process touches a different sink cell. Furthermore, in (e), we show the watershed boundary formed by the interface of cells belonging to different sinks.

We tested the IPBA method on Earth (in northcentral Wyoming) and compared IPBA-derived watershed boundary and that derived from the standard flow-based algorithm in ArcGIS Pro. The result is shown in Figure S1(a). In general, both boundaries coincide with each other, with the exception at the edge of the grid and a few minor differences in the interior. The IBPA does a good job in extracting the watershed boundary along the topographic ridge lines. An example of applying IPBA to Mars is shown in Figure S1(b). The boundary also generally follow topographic ridge lines. We also tested algorithm on different resolution data of the same area (30 m, 90 m, 250 m) and although there are minor differences between different resolutions (by a few pixels at most), the identified watershed boundary always follow the topographic ridge lines of the respective data.

2.3 Extracting Hack's Law exponent

To extract the Hack's Law exponent for each watershed, we first clipped the DEM using the watershed boundary, then used the standard flow-based method to derive flow accumulation in each cell (i.e., A in Eq. (1)) and the upstream flow length to drainage divide (L in Eq. (1)) using the flow accumulation and flow length tools, respectively, in ArcGIS Pro. Next, the least square approach was applied to fit the power law relationship to obtain the exponent h in Eq. (1). An example of watershed and Hack's Law exponent is shown in Fig. S2.

3 Results

3.1 Terrestrial

To provide context and aid in interpreting our results for Mars, we extracted the Hack's Law exponent for the conterminous US using the method and data (HUC6 watershed boundary) described above. The results from this effort are shown in Table 1 and Figure 2. Our results, although slightly different in values, are generally consistent with those of Yi et al. (2018). The h values are generally higher in humid regions than those in arid ones (Fig. 2A). Statistic t-test show that the difference of Hack's law exponents between the humid and arid regions are statistically significant ($p<0.0001$, two-tail).

Table 1. Statistics of Hack's Law exponent for conterminous US

Categories (# of basins)	Mean	Median	Standard deviation
All (350)	0.537	0.533	0.065
Arid[1] (101)	0.511	0.516	0.044
Humid[1] (249)	0.548	0.541	0.069
Cold Spots[2] (42)	0.483	0.486	0.048
Cold Spots w/o Great Lakes basins (31)	0.481	0.471	0.037

Categories (# of basins)	Mean	Median	Standard deviation
Hot Spots[2] (59)	0.603	0.579	0.100
Hot Spots w/o long Mississippi basins (55)	0.580	0.576	0.044

Note: 1. Arid is defined as area with average logarithm of aridity index less than -0.5 (Yi et al., 2018); the rest is defined as humid. 2. For Hot Spots and Cold Spots, see Figure 2(B).

We conducted spatial autocorrelation analysis (Global Moran's I) of h over conterminous US using ArcGIS Pro software (ESRI, n.d.-b). The null hypothesis is that the spatial distribution of h is random, i.e., h is spatially uncorrelated. The analysis generated a Moran's Index of 0.41, a z-score of 15.89 and a p-value of <0.0001, which means that the distribution is highly clustered and the null hypothesis can be safely rejected. This makes sense, because we know on Earth fluvial processes are primarily responsible for the formation of drainage systems.

We also conducted Hot Spot Analysis (Getis-Ord Gi*) with False Discovery Rate (FDR) Correction applied (ESRI, n.d.-a). This tool identifies statistically significant spatial clusters of high values (hot spots) and low values (cold spots). The FDR is a more stringent condition for statistical significance. The result is shown in Fig. 2(B). We will describe our observation of the patterns and offer our interpretation. The hot spots are generally located at: (1) slope area transitioning from High Plains to Central Lowland area (Hunt, 1967), (2) the coastal plains around the lower Mississippi valley, and (3) the highly dissection Appalachian Plateau and Valley and Ridge Provinces (Hunt, 1967). The cold spots are generally located at: (4) the Great Lakes region and (5) the Basin and Range Province and Colorado Plateau (Hunt, 1967), a generally very arid region. We believe areas (2) and (4) are artifacts of flat basins of the Great Lakes and a few long and thin basins right around the river itself in the lower Mississippi valley. The high values in areas (1) and (3) are likely caused by the fluvial erosion that elongated the watershed in the downslope direction. The low values in area (5) is related the arid climate and/or structure control of basin and range. The descriptive statistics of h in these areas and those excluding the artifacts are shown in Table 1.

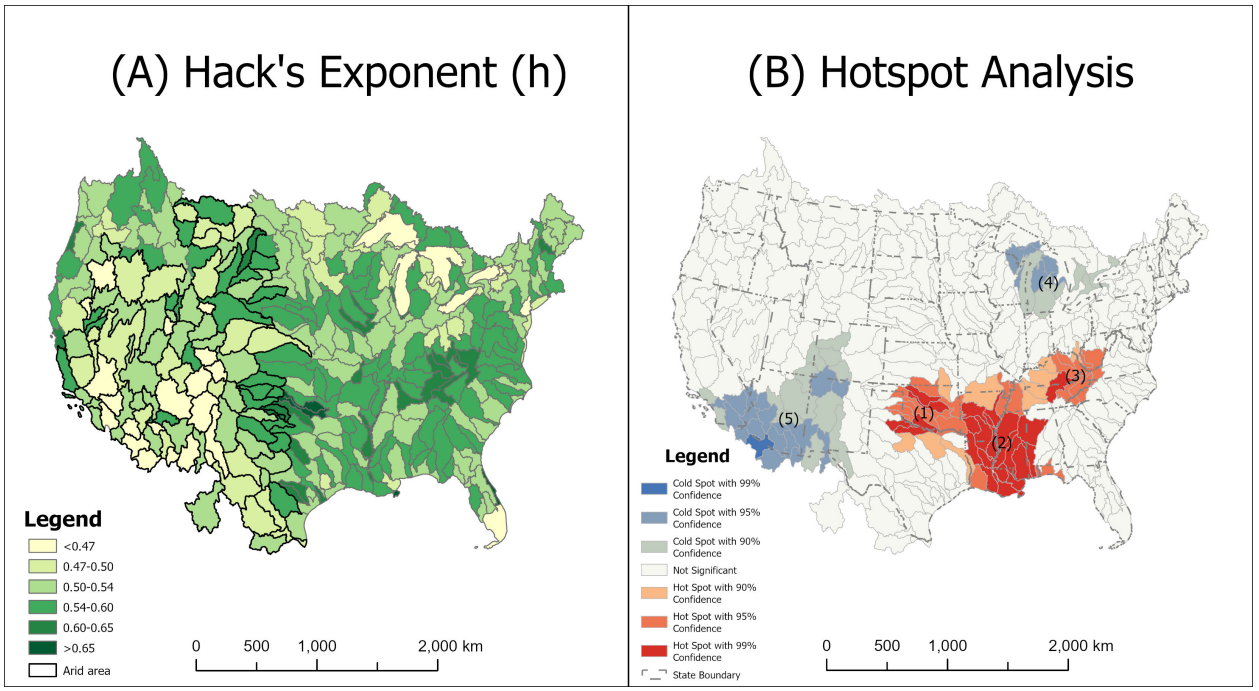

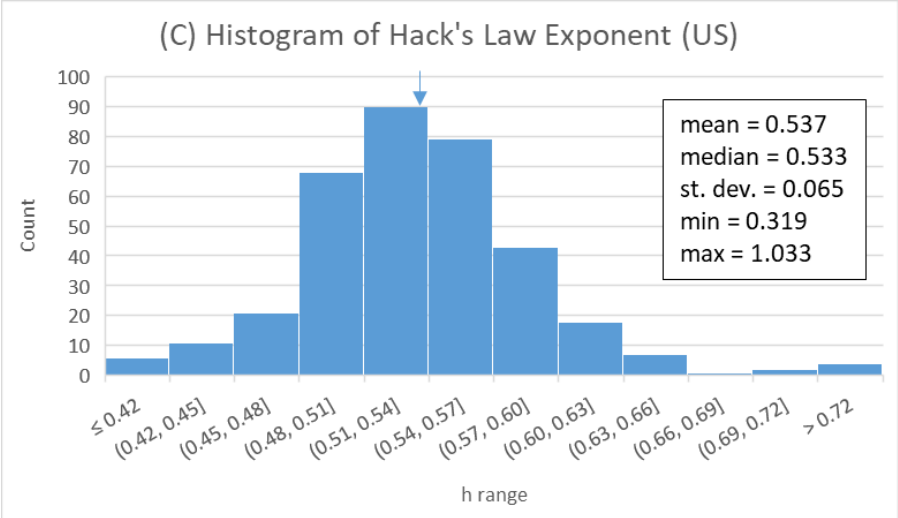

Figure 2. (A) Distribution of Hack's Law exponent h of conterminous US. Arid area (bold outline) is defined as basins with average logarithm of aridity index less than -0.5 (Yi et al., 2018). (B) Hotspot Analysis of h. (C) Histogram of h for conterminous US (arrow points to approximate mean value).

3.2 Mars

Fig. 3(a) shows the watershed boundary extracted from IPBA method along

with mapped VN and MOLA topography in the background. Watersheds on the edge of the DEM were removed from analysis because of the edge effect that forms the artificial straight boundaries (66 watersheds). The remaining total of 2563 watersheds were analyzed. Fig. 3(b) shows spatial distribution of h and Fig. 3(c) shows the histogram of h along with general descriptive statistics. The histogram is roughly normally distributed with a longer tail in the low value end than its terrestrial counterpart (Fig. 2c). The Martian mean value (0.472) is lower than that of US (0.537) and majority of values are between 0.4 and 0.6. The mean Martian value is similar to that of the cold spot value in the US arid area (0.48 with or without artifact areas, Table 1).

Spatial autocorrelation analysis (Global Moran's I) of h on Mars with the same null hypothesis (that the spatial distribution of h is random) generated a Moran's Index of 0.055, a z-score of 5.65 and p-value of <0.0001, which also indicates that the distribution is clustered and the null hypothesis can be safely rejected (ESRI, n.d.-b). This result suggests that the processes responsible for the VN formation on Mars were not random.

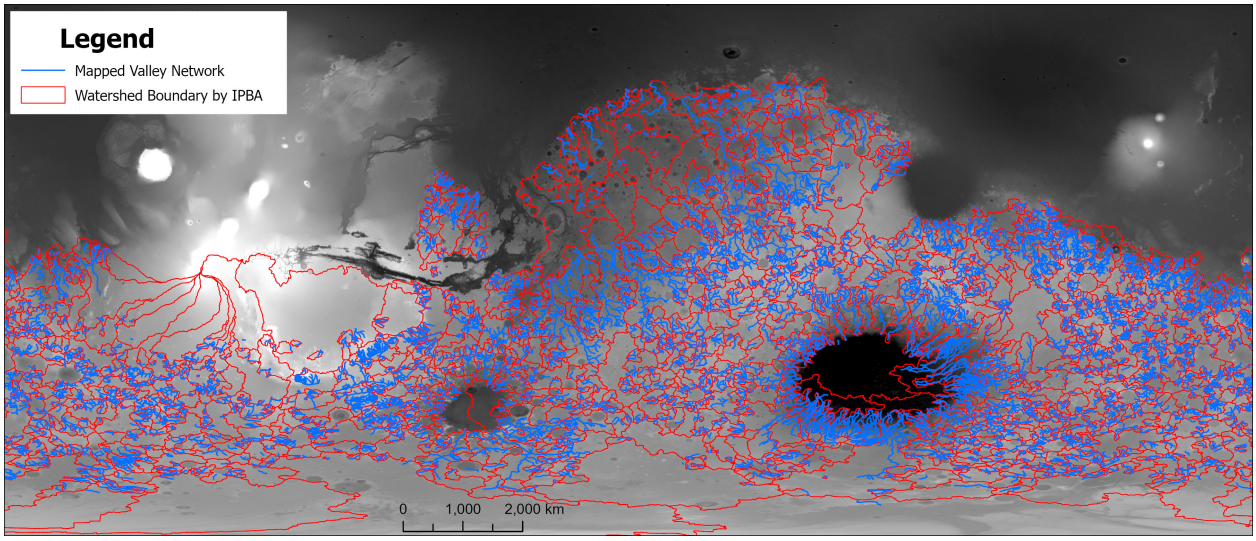

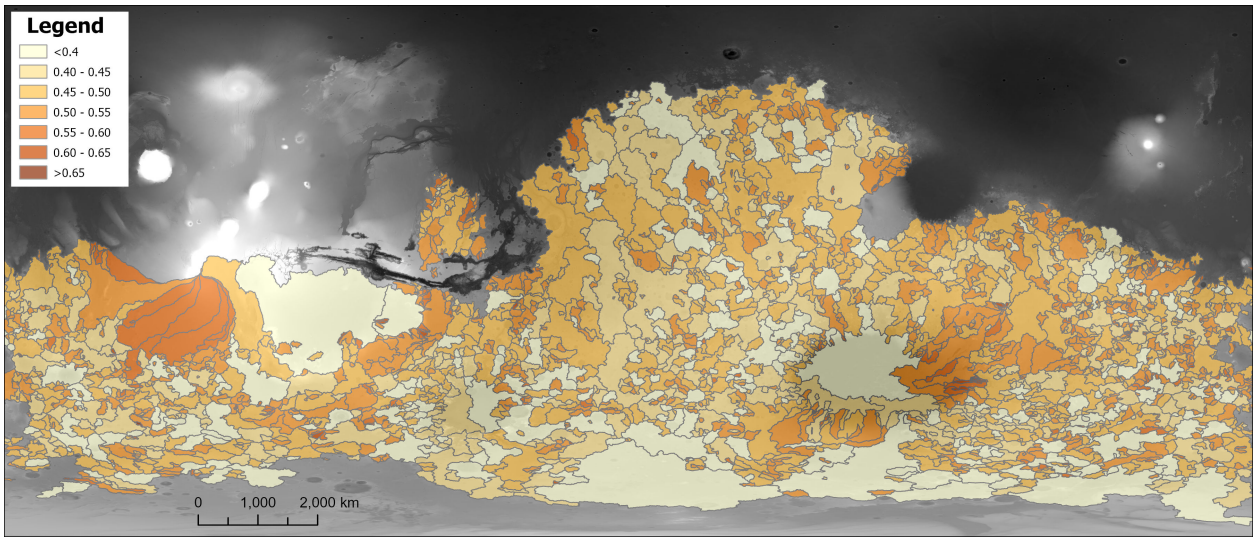
Legend
<0.4
0.40 - 0.45
0.45 - 0.50
0.50 - 0.55
0.55 - 0.60
0.60 - 0.65
>0.65
0
1,000
2,000 km

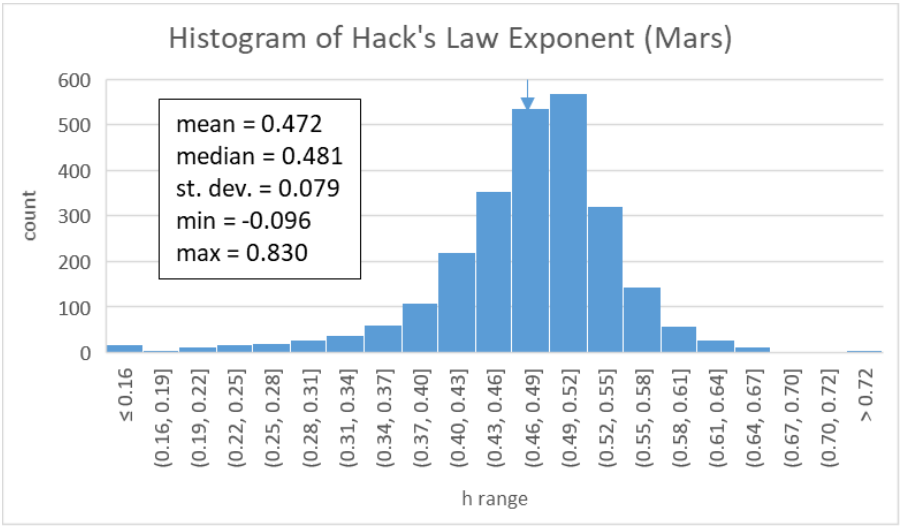
Histogram of Hack's Law Exponent (Mars)
mean = 0.472
median = 0.481
st. dev. = 0.079
min = -0.096
max = 0.830
count
600
500
400
300
200
100
0
≤ 0.16
(0.16, 0.19]
(0.19, 0.22]
(0.22, 0.25]
(0.25, 0.28]
(0.28, 0.31]
(0.31, 0.34]
(0.34, 0.37]
(0.37, 0.40]
(0.40, 0.43]
(0.43, 0.46]
(0.46, 0.49]
(0.49, 0.52]
(0.52, 0.55]
(0.55, 0.58]
(0.58, 0.61]
(0.61, 0.64]
(0.64, 0.67]
(0.67, 0.70]
(0.70, 0.72]
> 0.72
h range

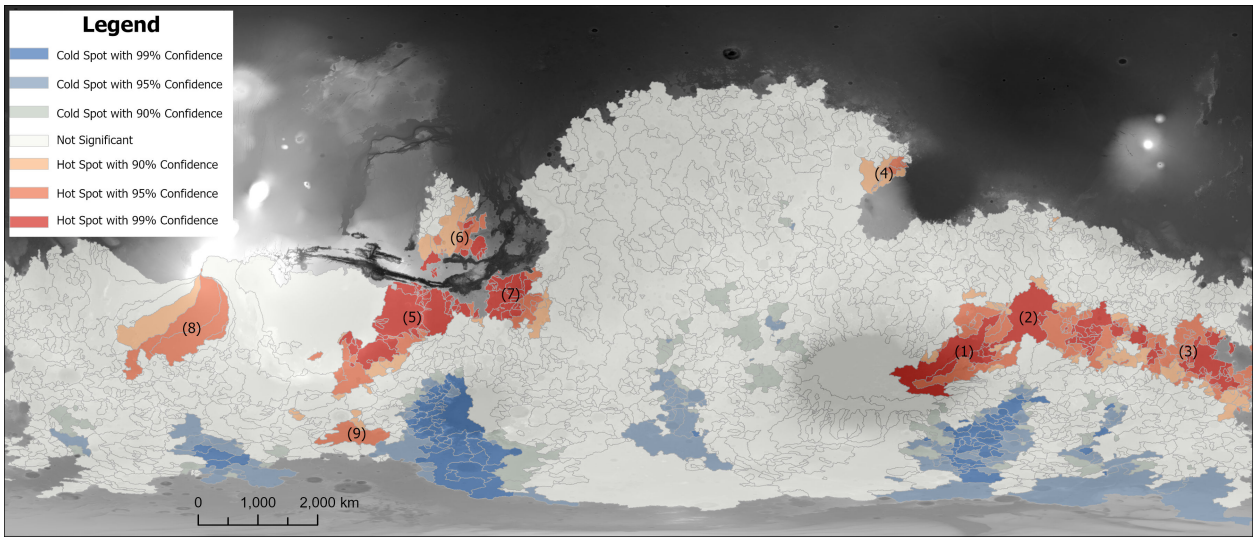

Figure 3. (a) Watershed boundary derived from IPBA along with mapped VN and MOLA DEM (shown in the background); (b) Spatial distribution of Hack's Law exponent h (note: h is derived using 200 m resolution blended MOLA-HRSC DEM based on watersheds shown in (a)) (c) histogram of h (arrow points to approximate mean value). (d) Hot spot analysis of h. See text for more details.

We also conducted similar Hot Spot Analysis (Getis-Ord Gi*) with False Discovery Rate (FDR) Correction applied (ESRI, n.d.-a). The result is shown in Fig. 3(d). Our observation and interpretation follows. Area (1) is located on a long topographic slope toward the Hellas basin. It is characterized by long, nearly parallel drainage with few tributaries. The region from parts of areas (1) & (2) are volcanic terrain (Early Hesperian volcanic unit (eHv), Late Hesperian volcanic unit (lHv), Hesperian volcanic edifice unit (Hve), Noachian volcanic edifice unit (Nve), and Late Noachian edifice unit (lNe)). Some of the drainage here is centripetal, and again generally poorly branched. Area (3) are mostly areas with large flat basins with few channels surrounded by limited channel networks draining into the basins. Some of the basins near (3) hosted a large upland lake that overflowed to form Ma'adim Vallis. The valleys are mostly relatively short and unbranched. Area (4) is also mostly eHv unit, along with some Middle Noachian highland unit (mNh). Area (5) is volcanic plains (eHv, Late Noachian volcanic unit (lNv), Nve), disrupted by grabens and wrinkle ridges. Valley networks are irregular and very localized. Area (6) is cratered, but affected by outflow channel development. Area (7) is broken up by development of chaotic terrain and thus fragmentary valleys. Area (8) is located in Daedalia Planum featuring solidified lava flows on the south-east slope of Arsia Mons. Area (9) is located on a mNh unit and Hesperian polar unit (Hp) (Tanaka et al., 2014). So overall, these high value areas are related to the underlying topography and appear to be influenced by volcanic lava flows and structures. The

co-location of these hot spots with volcanic units lends possible support to the idea that the early warm climate of Mars may be episodically triggered by brief and strong volcanic activity and associated outgassing of greenhouse gasses and aerosols (Halevy & Head, 2014).

The cold spot (blue) areas are mostly in Early, Middle, and Late Noachian highland units (eNh, mNh, lNh), along with some Amazonian and Hesperian impact units (Ahi) (Tanaka et al., 2014). They are consistently located farther in the south in the high latitude region. We interpret this as consistent with an early warm climate scenario that involved a northern ocean and hydrologic cycle; these areas are farthest away from the ocean water source and thus would be driest with lowest h values. The valley networks here may also have been strongly degraded by mid-latitude ice and dust accumulation and glacial activity.

The statistics of h values of all basins and different categories of hot/cold spots are summarized in Table 2. The majority of the basins in the non-hot/cold spots categories has mean and median values (0.47, 0.48) similar to those of cold spots on Earth (i.e., in arid areas and basin and range province in the US) (cf Table 1). Even those hot spots on Mars only have values (0.51) similar to those of arid area in the US. This suggests that the climate of early Mars was more arid than the current western US. Alternatively some structural control or impact cratering may have frustrated the full development of fluvial systems, leading the lower h value on Mars. It could also be the result of the combined effect of an arid climate and structure/impact control. However, we favor the arid climate interpretation because spatial distribution of cold spots is consistent with an early warm climate that had a northern ocean and hydrologic cycle.

Table 2. Statistics of Hack's Law exponent for Mars

Categories (# of basins)	Mean	Median	Standard deviation
All (2562)	0.472	0.481	0.079
Cold Spots (282)	0.427	0.445	0.088
Hot Spots (376)	0.516	0.512	0.064
Non-hot/cold spots (1904)	0.470	0.481	0.076

4 Conclusions

We used a parameter free method to delineate watersheds globally on Mars based on mapped VNs and then extracted their Hack's Law exponent (h). For comparison, we also extracted h for conterminous US on Earth. For both planets, the spatial statistics show that the underlying processes leading to the spatial pattern of h distribution were not random. The hot spot analysis revealed statistically significant high values and low values that are clustered in certain locations. For US, the low values (cold spots) are related to the arid climate and/or basin and range structure. The high values are likely caused by the

fluvial erosion that elongated the watershed in the downslope direction. The hot spots of h on Mars are likely related to the underlying topography and influenced by volcanic lava flows and structures, possibly supporting volcanically triggered episodic warm climate. The cold spots of h are all located in the south, consistent with an early warm climate scenario that likely involved a northern ocean and active hydrologic cycle. The overall Mars mean and median h values are lower than their US counterparts and most similar to those of the cold spots in the US (Fig. 3 and Table 1). The wide distribution of h with the majority value ranging from 0.4 to 0.6 on a global scale also suggest that VNs on Mars was most likely formed by fluvial processes. These results are most consistent with an early Mars climate that's warm and arid, which could be episodic, but with enough precipitation from hydrologic cycles involving a northern ocean to carve the valleys. This interpretation is consistent with a number of other recent geomorphic studies (e.g., Cang & Luo, 2019) and climate models (e.g., Kamada et al., 2021; Ramirez et al., 2020).

Acknowledgments

There is no real or perceived financial conflicts of interests for any author. This research is supported by NASA MDAP funding (award no. 80NSSC21K1087, to WL, AH, and RC) and Edson Queiroz Foundation (to EO and RP). We thank Yaxiong Shao and Jichao Fang for help with data processing.

Open Research

Almost all data used in this study are publically available. The SRTM 90-m Digital Elevation Database v4.1 can be downloaded from https://cgiarcsi.community/data/srtm-90m-digital-elevation-database-v4-1/. The US watershed boundary can be downloaded from https://www.usgs.gov/national-hydrography/watershed-boundary-dataset. The Global Aridity Index and Potential Evapotranspiration Climate Database can be downloaded from https://cgiarcsi.community/2019/01/24/global-aridity-index-and-potential-evapotranspiration-climate-database-v2/. MOLA DEM at 463 m resolution can be downloaded from https://astrogeology.usgs.gov/search/map/Mars/GlobalSurveyor/MOLA/Mars_MGS_MOLA_DEM_mosaic_global_463m. The HRSC and MOLA Blended Digital Elevation Model at 200 m can be downloaded at https://astrogeology.usgs.gov/search/map/Mars/Topography/HRSC_MOLA_Blend/Mars_HRSC_MOLA_BlendDEM_Global_200mp_v2. The mapped valley network data is from a previous publication (Matsubara et al., 2013).

The IPBA software code is available on GitHub (https://github.com/erneson/IPBA). The Mars watershed boundary shapefile data derived from IPBA is in the process of being archived in Zenodo (https://zenodo.org/) and a copy is temporarily uploaded as Supporting Information for review purposes.

References

Baker, V. R., Hamilton, C. W., Burr, D. M., Gulick, V. C., Komatsu, G., Luo, W., et al. (2015). Fluvial geomorphology on Earth-like planetary surfaces: A review. *Geomorphology*, *245*, 149–182. https://doi.org/10.1016/j.geomorph.2015.05.002Buffo, J. J., Ojha, L., Meyer, C. R., Ferrier, K. L., & Palucis, M. C. (2022). Revisiting subglacial hydrology as an origin for Mars' valley networks. *Earth and Planetary Science Letters*, *594*, 117699. https://doi.org/10.1016/j.epsl.2022.117699Cang, X., & Luo, W. (2019). Noachian climatic conditions on Mars inferred from valley network junction angles. *Earth and Planetary Science Letters*, *526*, 115768. https://doi.org/10.1016/j.epsl.2019.115768Caprarelli, G., & Wang, B. Y. (2012). Wet Mars implications of revised scaling calculations for Evros Vallis. *Australian Journal of Earth Sciences*, *59*(2), 263–276. https://doi.org/10.1080/08120099.2012.622294Craddock, R. A., & Howard, A. D. (2002). The case for rainfall on a warm, wet early Mars. *Journal of Geophysical Research*, *107(E11)*, Doi:10.1029/2001je001505.Dodds, P. S., & Rothman, D. H. (2000). Scaling, Universality, and Geomorphology. *Annual Review of Earth and Planetary Sciences*, *28*(1), 571–610. https://doi.org/10.1146/annurev.earth.28.1.571Ehlmann, B. L., Mustard, J. F., Murchie, S. L., Bibring, J.-P., Meunier, A., Fraeman, A. A., & Langevin, Y. (2011). Subsurface water and clay mineral formation during the early history of Mars. *Nature*, *479*(7371), 53–60. https://doi.org/10.1038/nature10582ESRI. (n.d.-a). *ArcGIS Pro: Hot Spot Analysis (Getis-Ord Gi*) (Spatial Statistics)(https://pro.arcgis.com/en/pro-app/latest/tool-reference/spatial-statistics/hot-spot-analysis.htm)*. ESRI. Retrieved from https://pro.arcgis.com/en/pro-app/latest/tool-reference/spatial-statistics/hot-spot-analysis.htmESRI. (n.d.-b). *ArcGIS Pro: Spatial Autocorrelation (Global Moran's I) (Spatial Statistics)(https://pro.arcgis.com/en/pro-app/latest/tool-reference/spatial-statistics/spatial-autocorrelation.htm)*. ESRI. Retrieved from https://pro.arcgis.com/en/pro-app/latest/tool-reference/spatial-statistics/spatial-autocorrelation.htmFastook, J. L., & Head, J. W. (2015). Glaciation in the Late Noachian Icy Highlands: Ice accumulation, distribution, flow rates, basal melting, and top-down melting rates and patterns. *Planetary and Space Science*, *106*, 82–98. https://doi.org/10.1016/j.pss.2014.11.028Fehr, E., Andrade Jr, J. S., da Cunha, S. D., da Silva, L. R., Herrmann, H. J., Kadau, D., et al. (2009). New efficient methods for calculating watersheds. *Journal of Statistical Mechanics: Theory and Experiment*, *2009*(09), P09007. https://doi.org/10.1088/1742-5468/2009/09/P09007Fergason, R. L., Hare, T. M., & Laura, J. (2018). HRSC and MOLA Blended Digital Elevation Model at 200m v2. Retrieved from http://bit.ly/HRSC_MOLA_Blend_v0Forget, F., Wordsworth, R., Millour, E., Madeleine, J.-B., Kerber, L., Leconte, J., et al. (2013). 3D modelling of the early martian climate under a denser CO2 atmosphere: Temperatures and CO2 ice clouds. *Icarus*, *222*(1), 81–99. https://doi.org/10.1016/j.icarus.2012.10.019Gough, D. O. (1981). Solar interior structure and luminosity variations. *Solar Physics*, *74*(1), 21–34. https://doi.org/10.1007/BF00151270Grau Galofre, Jellinek, A. M., & Osinski, G. R. (2020). Valley formation on early Mars by subglacial and fluvial erosion. *Nature Geoscience*, *13*(10), 663–668. https://doi.org/10.1038/s41561-020-0618-

xGrau Galofre, Whipple, K. X., Christensen, P. R., & Conway, S. J. (2022). Valley Networks and the Record of Glaciation on Ancient Mars. *Geophysical Research Letters*, *49*(14). https://doi.org/10.1029/2022GL097974Gulick, V. C. (1998). Magmatic intrusions and a hydrothermal origin for fluvial valleys on Mars. *Journal of Geophysical Research*, *103*, 19,365-19,387.Hack, J., Tilton. (1957). *Studies of longitudinal stream profiles in Virginia and Maryland* (SHORTER CONTRIBUTIONS TO GENERAL GEOLOGY). Washington 25, D. C.: United States Geological Survey. Retrieved from https://pubs.usgs.gov/pp/0294b/report.pdfHalevy, I., & Head, J. W. (2014). Episodic warming of early Mars by punctuated volcanism. *Nature Geoscience*, *7*(12), 865–868. https://doi.org/10.1038/ngeo2293Hunt, C. B. (1967). *Physiography of the United States*. San Francisco: W.H. Freeman.Hynek, B. M., & Phillips, R. J. (2003). New data reveal mature, integrated drainage systems on Mars indicative of past precipitation. *Geology*, *31*, 757–760.Jarvis, A., Reuter, H. I., Nelson, A., & Guevara, E. (2008). Hole-filled SRTM for the globe Version 4, available from the CGIAR-CSI SRTM 90m Database. Retrieved from https://cgiarcsi.community/data/srtm-90m-digital-elevation-database-v4-1/Kamada, A., Kuroda, T., Kasaba, Y., Terada, N., & Nakagawa, H. (2021). Global climate and river transport simulations of early Mars around the Noachian and Hesperian boundary. *Icarus*, *368*, 114618. https://doi.org/10.1016/j.icarus.2021.114618Luo, W., & Stepinski, T. F. (2009). Computer-generated global map of valley networks on Mars. *Journal of Geophysical Research-Planets*, *114*.Matsubara, Y., Howard, A. D., & Gochenour, J. P. (2013). Hydrology of early Mars: Valley network incision: HYDROLOGY OF EARLY MARS: VALLEY INCISION. *Journal of Geophysical Research: Planets*, *118*(6), 1365–1387. https://doi.org/10.1002/jgre.20081Oliveira, E. A., Pires, R. S., Oliveira, R. S., Furtado, V., Herrmann, H. J., & Andrade, J. S. (2019). A universal approach for drainage basins. *Scientific Reports*, *9*(1), 9845. https://doi.org/10.1038/s41598-019-46165-0Penido, J. C., Fassett, C. I., & Som, S. M. (2013). Scaling relationships and concavity of small valley networks on Mars. *Planetary and Space Science*, *75*, 105–116. https://doi.org/10.1016/j.pss.2012.09.009Ramirez, R. M., & Craddock, R. A. (2018a). The geological and climatological case for a warmer and wetter early Mars. *Nature Geoscience*, *11*(4), 230–237. https://doi.org/10.1038/s41561-018-0093-9Ramirez, R. M., & Craddock, R. A. (2018b). The geological and climatological case for a warmer and wetter early Mars. *Nature Geoscience*, *11*(4), 230–237. https://doi.org/10.1038/s41561-018-0093-9Ramirez, R. M., Craddock, R. A., & Usui, T. (2020). Climate Simulations of Early Mars With Estimated Precipitation, Runoff, and Erosion Rates. *Journal of Geophysical Research: Planets*, *125*(3). https://doi.org/10.1029/2019JE006160Rigon, R., Rinaldo, A., Rodriguez-Iturbe, I., Bras, R. L., & Ijjasz-Vasquez, E. (1993). Optimal channel networks: A framework for the study of river basin morphology. *Water Resources Research*, *29*(6), 1635–1646. https://doi.org/10.1029/92WR02985Smith, D. E., Zuber, M. T., Frey, H. V., Garvin, J. B., Head, J. W., Muhleman, D. O., et al. (2001). Mars Orbiter Laser Altimeter: Experiment summary after the first year of global mapping

of Mars. *Journal of Geophysical Research: Planets*, *106*(E10), 23689–23722. https://doi.org/10.1029/2000JE001364Som, S. M., Montgomery, D. R., & Greenberg, H. M. (2009). Scaling relations for large Martian valleys. *Journal of Geophysical Research*, *114*(E2). https://doi.org/10.1029/2008JE003132Tanaka, K. L., Skinner, J. A. Jr., Dohm, J. M., Irwin, R. P., III, Kolb, E. J., Fortezzo, C. M., et al. (2014). *Geologic map of Mars: U.S. Geological Survey Scientific Investigations Map 3292, scale 1:20,000,000.*Trabucco, Antonio, & Zomer, Robert. (2022). Global Aridity Index and Potential Evapotranspiration (ET0) Climate Database v3 [Data set]. figshare. https://doi.org/10.6084/M9.FIGSHARE.7504448.V4Turbet, M., & Forget, F. (2019). The paradoxes of the Late Hesperian Mars ocean. *Scientific Reports*, *9*(1). https://doi.org/10.1038/s41598-019-42030-2Vincent, L., & Soille, P. (1991). Watersheds in digital spaces: an efficient algorithm based on immersion simulations. *IEEE Transactions on Pattern Analysis and Machine Intelligence*, *13*(6), 583–598. https://doi.org/10.1109/34.87344Wilkinson, D., & Willemsen, J. F. (1983). Invasion percolation: a new form of percolation theory. *Journal of Physics A: Mathematical and General*, *16*(14), 3365–3376. https://doi.org/10.1088/0305-4470/16/14/028Wordsworth, R., Forget, F., Millour, E., Head, J. W., Madeleine, J.-B., & Charnay, B. (2013). Global modelling of the early martian climate under a denser CO2 atmosphere: Water cycle and ice evolution. *Icarus*, *222*(1), 1–19. https://doi.org/10.1016/j.icarus.2012.09.036Wordsworth, R. D. (2016a). The Climate of Early Mars. *Annual Review of Earth and Planetary Sciences*, *44*(1), 381–408. https://doi.org/10.1146/annurev-earth-060115-012355Wordsworth, R. D. (2016b). The Climate of Early Mars. *Annual Review of Earth and Planetary Sciences*, *44*(1), 381–408. https://doi.org/10.1146/annurev-earth-060115-012355Yi, R. S., Arredondo, Á., Stansifer, E., Seybold, H., & Rothman, D. H. (2018). Shapes of river networks. *Proceedings of the Royal Society A: Mathematical, Physical and Engineering Sciences*, *474*(2215), 20180081. https://doi.org/10.1098/rspa.2018.0081

Supplement Material

Supplement Material

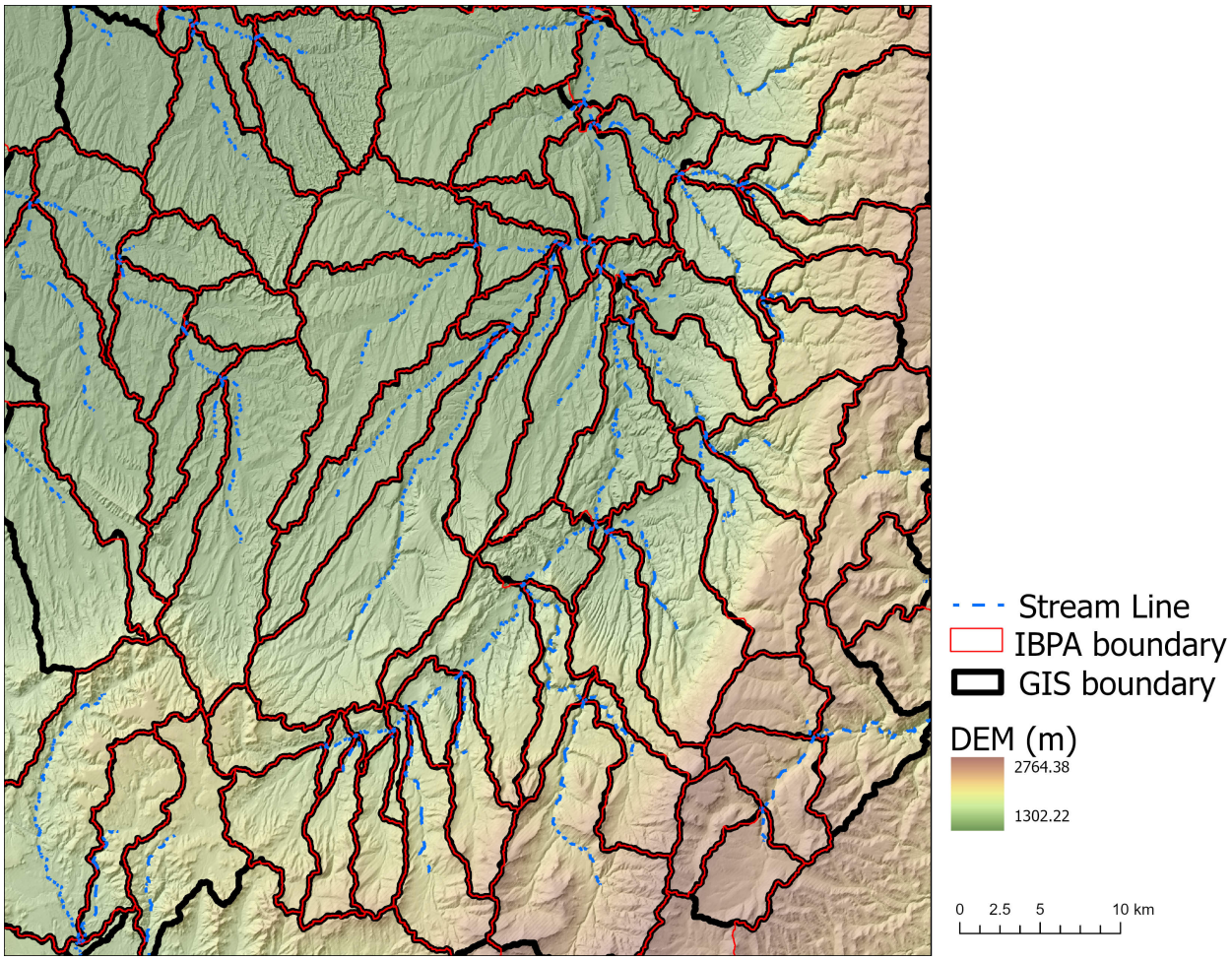
Stream Line
IBPA boundary
GIS boundary
DEM (m)
2764.38
1302.22
0
2.5
5
10 km

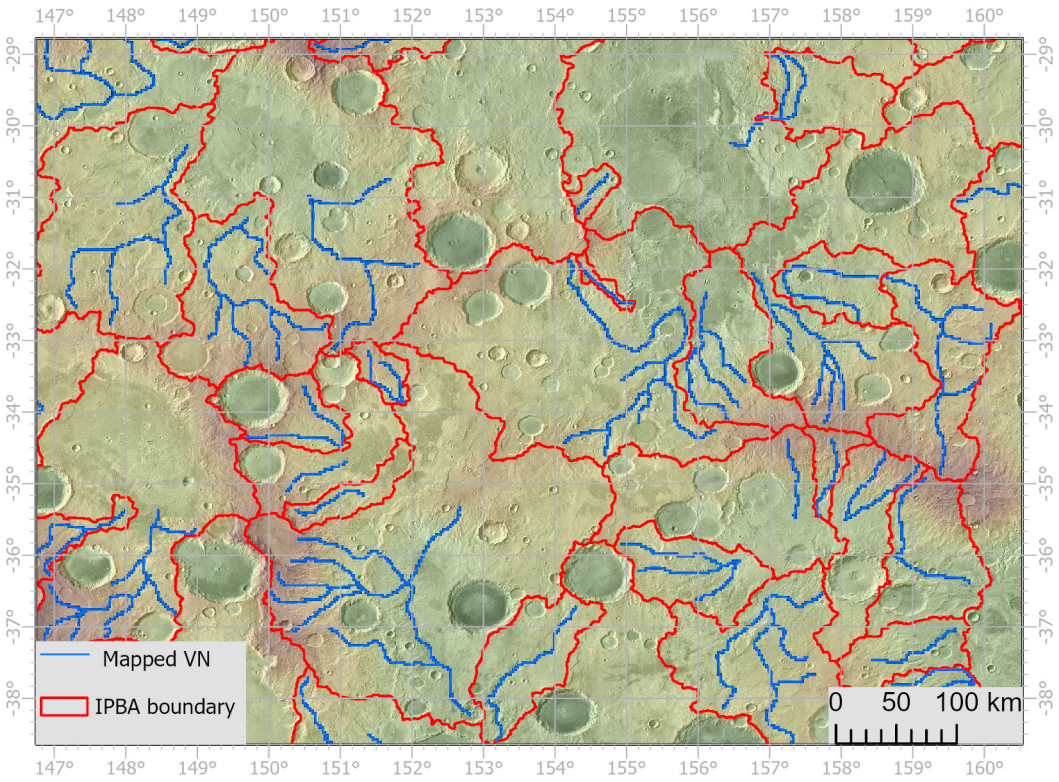

Figure S1. (a) Comparison of watershed boundary derived from IPBA method and standard flow-based method in GIS draining to the same set of stream lines in northcentral Wyoming (center of the figure is roughly located at 107.4°W, 43.7°N). (b) Example of watershed boundary draining to mapped VN on Mars derived from IPBA method. The background is the THEMIS day time image mosaic tinted with MOLA elevation (brown color is high and green is low).

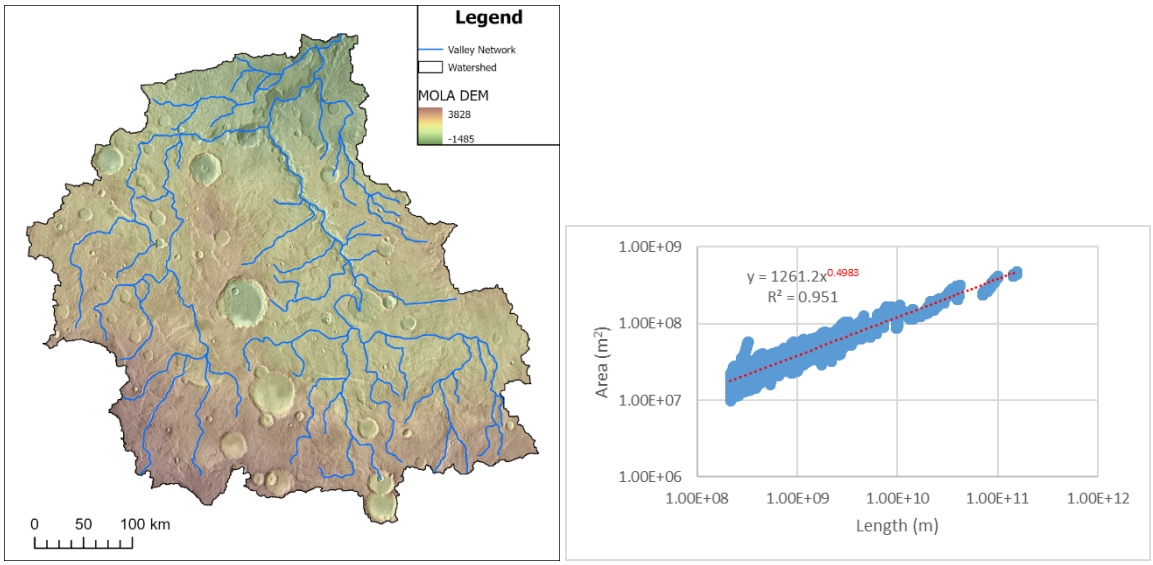

Figure S2. Example watershed and Hack's Law exponent.